

Momentum and energy dissipation of hot electrons in a Pb/Ag(111) quantum well system

Florian Haag ^{1,2,*}, Tobias Eul ¹, Lisa Grad ^{1,†}, Norman Haag ¹, Johannes Knippertz,¹ Stefan Mathias ^{3,4},
Mirko Cinchetti ⁵, Martin Aeschlimann,¹ and Benjamin Stadtmüller ^{1,6,‡}

¹*Department of Physics and Research Center OPTIMAS, TU Kaiserslautern, Erwin-Schroedinger-Straße 46, 67663 Kaiserslautern, Germany*

²*Graduate School of Excellence Materials Science in Mainz, Erwin-Schroedinger-Straße 46, 67663 Kaiserslautern, Germany*

³*I. Physikalisches Institut, Georg-August-Universität Göttingen, Friedrich-Hund-Platz 1, 37077 Göttingen, Germany*

⁴*International Center for Advanced Studies of Energy Conversion (ICASEC),
Georg-August-Universität Göttingen, 37077 Göttingen, Germany*

⁵*Experimentelle Physik VI, Technische Universität Dortmund, 44221 Dortmund, Germany*

⁶*Institute of Physics, Johannes Gutenberg University Mainz, Staudingerweg 7, 55128 Mainz, Germany*



(Received 10 February 2021; revised 7 June 2021; accepted 27 August 2021; published 15 September 2021)

The band structure of multilayer systems plays a crucial role for the ultrafast hot carrier dynamics at interfaces. Here, we study the energy- and momentum-dependent quasiparticle lifetimes of excited electrons in a highly ordered Pb monolayer film on Ag(111) prior and after the adsorption of a monolayer of 3,4,9,10-perylene-tetracarboxylic dianhydride (PTCDA). Using time-resolved two-photon momentum microscopy with femtosecond visible light pulses, we show that the electron dynamics of the Pb/Ag(111) quantum well system is largely dominated by two types of scattering processes: (i) isotropic intraband scattering processes within the quantum well state (QWS) and (ii) isotropic interband scattering processes from the p_z -like QWS into the Pb $p_{x/y}$ band. In the latter case, the Pb QWS acts as an electron source for the momentum space refilling process of the Pb $p_{x/y}$ band. This conclusion is confirmed by the modification of the band structure and the quasiparticle dynamics of the Pb/Ag(111) bilayer film after the adsorption of PTCDA. We find both an adsorption-induced suppression of the QWS itself as well as of the refilling process into the Pb $p_{x/y}$ band. Our study hence demonstrates the isotropic nature of the momentum-dependent scattering processes of metallic bilayer systems and uncovers a new possibility to selectively tune and control scattering processes occurring in quantum (well) materials by the adsorption of organic molecules.

DOI: [10.1103/PhysRevB.104.104308](https://doi.org/10.1103/PhysRevB.104.104308)

I. INTRODUCTION

Interfaces between functional materials are important building blocks for the next generation of nanosized optoelectronic, photonic, and spintronic devices [1,2]. They do not only determine the efficiency of charge and spin transport through the device structure but can also mediate application-relevant functionalities, such as spin filtering or charge-to-spin and spin-to-charge conversion processes [3–6]. These functionalities are thereby closely linked to the interfacial band structure and the corresponding ultrafast carrier dynamics at these interfaces.

For this reason, countless studies focused on the (spin-dependent) single particle electron dynamics in ultrathin metallic or molecular films on surfaces. In this way, angle-resolved photoelectron spectroscopy [7–10], scanning tunneling microscopy [11–14], as well as time-resolved spectroscopy techniques [15–35] have laid the foundation for today's understanding of the dominating energy and

momentum dissipation mechanisms of excited carriers at surfaces, interfaces, and in bulk materials. The most direct way to experimentally quantify the ultrafast electron dynamics is to determine the quasiparticle lifetime of optically excited electrons in time-resolved two-photon photoemission spectroscopy (tr-2PPE) [36–42]. For heterostructures without structural order or for low excitation energies, the electron lifetime only depends on the energy of the excited carriers and is determined by inelastic electron-electron scattering processes [42–44]. Energy- and momentum-dependent lifetimes can only be observed for material systems with well-defined (interfacial) band structures exhibiting, for instance, quantum well states, image potential states or modified surface states [20,24,40,45–54]. For such cases, electron-phonon or electron-defect scattering leads to both energy and momentum dissipation of excited electrons, which are typically classified as inter- or intraband scattering processes [20,24,55–57].

To gain further insights into the inter- or intraband scattering processes at interfaces, we turn to the single-particle electron dynamics of one layer of lead (Pb) grown on an Ag(111) single crystal surface [58,59]. This model system was selected as an exemplary case from the manifold of ultrathin metallic bilayer systems that can host quantum well states (QWSs) [17,19,20,24,55,59]. In the case of the Pb/Ag(111)

*f_haag@rhrk.uni-kl.de

†Current address: Department of Physics, University of Zürich, Winterthurerstrasse 190, 8057 Zürich, Switzerland.

‡bstadtmueller@physik.uni-kl.de

interface, the band structure reveals two distinct bands with different orbital character in the Pb layer: (i) a parabolic, free-electron-like QWS with parabolic dispersion in the center of the surface Brillouin zone and p_z orbital character and (ii) a second Pb band with $p_{x/y}$ orbital character [59]. These two bands are expected to dominate the ultrafast electron dynamics of such ultrathin Pb films.

Previous tr-2PPE studies of similar ultrathin Pb layers already proposed complex inter- and intraband scattering processes between different Pb-derived states [20,24] in a limited part of the surface Brillouin zone (either conducted without angular (momentum) resolution or along one high symmetry direction in momentum space). We build on these pioneering studies using time-resolved two-photon momentum microscopy (tr-2PMM) [60]. This approach combines the optical setup of a conventional tr-2PPE experiment with a photoemission electron microscope operated in momentum space mode, i.e., a momentum microscope [61–64]. Such a tr-2PMM experiment allows us to study inelastic as well as (quasi-) elastic inter- and intraband scattering processes in the entire accessible momentum space with a parallel detection scheme and in a fixed experimental geometry.

Our tr-2PMM experiments demonstrate that the electron dynamics of the Pb/Ag(111) bilayer system is dominated by isotropic scattering processes of electrons in the Pb layer. These scattering processes lead to an isotropic lifetime of the QWS of $\tau \approx 12$ fs in momentum space. The value of the quasiparticle lifetime within the QWS increases slightly when approaching the band minimum due to the reduced phase space for intraband scattering (electron-phonon scattering). Most importantly, we observe an isotropic interband scattering of electrons from the QWS into the Pb band with $p_{x/y}$ orbital character. This scattering process leads to a refilling of electrons into the Pb $p_{x/y}$ band that is responsible for an enhanced quasiparticle lifetime in this Pb $p_{x/y}$ band.

This conclusion is confirmed by the electron dynamics of the PTCDA/Pb/Ag(111) multilayer system which provides further evidence that the QWS acts as an electron source for the isotropic interband scattering in momentum space within the ultrathin Pb film.

II. EXPERIMENTAL DETAILS

A. Sample preparation

All experiments and the sample preparation procedures were performed under ultrahigh-vacuum conditions with a base pressure better than 1×10^{-9} mbar. The surface of the (111)-oriented silver crystal was cleaned by several cycles of argon ion bombardments and subsequent annealing at a temperature of $T_{\text{Sample}} = 730$ K. The cleanliness of the Ag(111) surface was verified by the width of the diffraction spots in low energy electron diffraction (LEED) measurements and the linewidth of the Shockley surface state at the $\bar{\Gamma}$ point in two-photon momentum microscopy. Afterwards, more than one monolayer Pb was evaporated onto the clean substrate at room temperature. Subsequent annealing for 10 min at 420 K leads to desorption of higher Pb layers resulting in a uniform single Pb layer on the Ag(111) surface [58,59]. The structural order of the Pb layer was checked

with LEED and momentum-resolved photoemission spectroscopy. The 3,4,9,10-perylene-tetracarboxylic dianhydride (PTCDA) monolayer film was prepared by thermal evaporation of PTCDA onto the Pb/Ag bilayer system at room temperature using a commercial evaporator. The coverage of the molecule PTCDA was controlled by the evaporation time and the flux of the evaporator. After the evaporation, the coverage of the PTCDA film was confirmed by comparing the total photoemission yield of the highest occupied molecular orbital of PTCDA on the Pb/Ag(111) bilayer to the one of PTCDA/Ag(111). We have selected this reference system since an ideal PTCDA monolayer film with a coverage of 1.0 ML can be prepared on Ag(111) by thermal desorption of a PTCDA multilayer film [65]. The structural order of the molecular film on top of the Pb layer was characterized by LEED as well as the existence and orientation of the characteristic emission pattern of the frontier molecular orbitals of PTCDA in momentum-resolved valence band photoemission spectroscopy [59,66]. The PTCDA film investigated here revealed all characteristic signatures that were recently reported by a comprehensive characterization study of the PTCDA/Pb/Ag(111) multilayer system [59].

B. Time-resolved two-photon momentum microscopy

The tr-2PMMs experiments were performed with a photoemission electron microscope (PEEM) operated in k -space mode. We used a time-of-flight detector as energy analyzer [64,67,68] for the experiments of the Pb/Ag(111) bilayer films and a double hemispherical analyzer [61–63] for the investigation of the PTCDA monolayer film on the Pb/Ag(111) bilayer system. Both microscopes are combined with optical beamlines for pump-probe spectroscopy [60]. As light sources, we used the second harmonics (SHG) of titanium-sapphire laser oscillators with a central wavelength of 800 nm (1.55 eV) for the fundamental emission line, sub 30 fs pulse width (FWHM), and a repetition rate of 80 MHz. The pulse duration of the SHG is smaller than 34 fs and was determined from the autocorrelation trace of the Cu(111) Shockley surface state [69,70]. The polarization of the SHG radiation was controlled by using a λ -half-wave plate. A mirror located within the PEEM optics was used for the nearly normal incidence angle measurements (4° incidence angle with respect to the surface normal) [71]. All experiments were conducted at room temperature.

The multidimensional data sets $I(k_x, k_y, E-E_F, \Delta t)$ were analyzed using the same approach as described in our previous work [60]: First, the momentum-resolved photoemission data of each energy were cutoff at the photoemission horizon to reduce the influence of pixels with marginal intensity in our photoemission data analysis. Then, the momentum-dependent lifetimes were determined by extracting autocorrelation curves at each remaining point in the momentum space for each intermediate state energy $E-E_F$. These traces were analyzed within the framework of optical Bloch equations which yields lifetimes in momentum space [69,72,73]. These lifetimes are plotted as color code in so-called lifetime maps, which reflect the lifetimes of electrons throughout the entire accessible momentum space in a

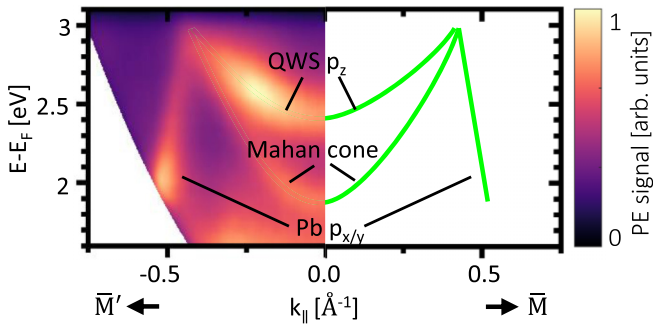


FIG. 1. Left: Energy vs momentum photoemission map of the excited states of the Pb/Ag(111) bilayer system along the $\overline{M'}\overline{\Gamma}$ direction. The dispersions of the Pb-derived QWS and the Pb $p_{x/y}$ band are illustrated in the band structure sketch on the right side.

tr-2PMM experiment. The relative experimental uncertainty of the quasiparticle lifetimes within a single tr-2PMM experiment is smaller than 1 fs. This value is estimated by an error analysis of the autocorrelation trace fitting using the optical Bloch equations as a fitting function. The very small experimental uncertainty is a direct result of the identical experimental conditions (in particular the FWHM of the laser pulses) that are used as identical input parameters for the analysis of the autocorrelation traces of the individual regions in energy and momentum space for a single data set. The relative uncertainty is hence largely determined by the signal-to-noise ratio of the autocorrelation traces. In contrast, the absolute experimental uncertainty of the quasiparticle lifetime is larger and can be estimated by ≈ 1 -2 fs. Note that these lifetimes do not necessarily reflect the pure intrinsic quasiparticle lifetime of the corresponding state in energy and momentum space but also contain signatures of energy- and momentum-dependent refilling processes.

III. RESULTS AND DISCUSSION

We start our discussion with the momentum-dependent hot electron dynamics of the bare Pb/Ag(111) bilayer system. All momentum microscopy data were obtained at room temperature.

The unoccupied band structure of the Pb/Ag(111) bilayer system is illustrated in Fig. 1. It is dominated by two Pb-derived states [59]: (i) a free-electron-like quantum well state (labeled QWS p_z) with p_z orbital character and (ii) a Pb-derived band (labeled Pb $p_{x/y}$) with $p_{x/y}$ orbital character and an apparently linear dispersion. This Pb $p_{x/y}$ band, however, also exhibits an electronlike parabolic dispersion but with its band minimum located in the occupied valence band structure ($E - E_F < -2$ eV) close to the border of the surface Brillouin zone [58]. The dispersion of the Pb $p_{x/y}$ band hence only appears linear in the small energy and momentum range investigated in our study. The third spectroscopic feature with parabolic dispersion (labeled Mahan cone) is not a band of the unoccupied Pb/Ag band structure, but can be attributed to a so-called Mahan cone transition [74,75] between sp -like bands of the Pb/Ag bilayer structure via a virtual intermediate state. Hence, this transition does not play a significant role

in the hot electron dynamics and thus will not be discussed further.

The energy- and momentum-dependent electron dynamics of the Pb $p_{x/y}$ band can be extracted from the tr-2PMM data in Fig. 2. They were obtained in a monochromatic (3.1 eV) 2PPE experiment in nearly normal incidence geometry with the in-plane electric field vector aligned along the k_x direction [see sketch in Fig. 2(a)]. In this geometry, the light pulses of the pump- and probe beam can only excite and probe states with predominant in-plane orbital character. This approach yields similar results as the more conventional photoemission experiments conducted in grazing incidence geometry with s -polarized light that is often used to determine the orbital character of surface and interface states. The in-plane character of the exciting light field is clearly reflected in the energy vs momentum cut along the $\overline{M'}\overline{\Gamma}\overline{M}$ direction in Fig. 2(b), which only shows the spectroscopic signature of the Pb $p_{x/y}$ band (marked by a green dotted line as a guide to the eye). The dispersion of this state is reflected in the constant energy (CE) maps in Fig. 2(c), which were recorded at three intermediate state energies of $E - E_F = 2.65, 2.85$ and 3.0 eV. The Pb-derived state appears as a ringlike feature with an azimuthal intensity distribution in all CE maps. The intensity modulation is the result of the in-plane orbital character and the p_{3m1} symmetry of the Pb superstructure on Ag(111).

The momentum-dependent quasiparticle lifetime of this state is displayed in three exemplary lifetime maps in Fig. 2(d), which were obtained at the same intermediate state energies as the CE intensity maps in Fig. 2(c). The color code of these lifetime maps represents the quasiparticle lifetime at each position in momentum space. They were obtained by extracting the time-dependent autocorrelation traces in well-defined regions in energy and momentum space and analyzing their line shape using optical Bloch equations as described in Ref. [60]. Exemplary autocorrelation traces of different regions in momentum space [marked in Fig. 2(c)] are shown as dots in Fig. 2(e), together with the two-pulse autocorrelation of the fs laser pulses (gray solid line).

All lifetime maps show momentum-independent quasiparticle lifetimes of only a few femtoseconds, which slightly increase when reducing the intermediate state energy towards the Fermi energy. In particular, the CE lifetime maps do not show any momentum space pattern that resembles the dispersion of the Pb $p_{x/y}$ band (marked by green half circles in Fig. 2(d) as a guide to the eyes). This observation indicates a neglectable intrinsic quasiparticle lifetime of the Pb $p_{x/y}$ band, i.e., the lifetime is indistinguishable from the lifetime of the homogeneous background of the Ag(111) crystal within the experimental uncertainty ($\tau_{SB} = 8.5 \pm 0.5$ fs, $\tau_{BG} = 8.2 \pm 0.5$ fs). This conclusion is also confirmed by the energy vs momentum lifetime map along the $\overline{M'}\overline{\Gamma}\overline{M}$ direction in Fig. 2(f), which does not show any pattern following the linear dispersion of the Pb $p_{x/y}$ band. The energy-dependent and momentum averaged quasiparticle lifetime is quantified in Fig. 2(g). It increases from $\tau \approx 6$ fs at $E - E_F = 3.0$ eV to $\tau \approx 9$ fs at $E - E_F = 1.8$ eV. Similar results were also obtained for reference tr-2PMM experiments with s -polarized laser light and grazing incidence geometry (65°) on the very same sample. In this geometry, the laser light also only exhibits an in-plane component of the electric field

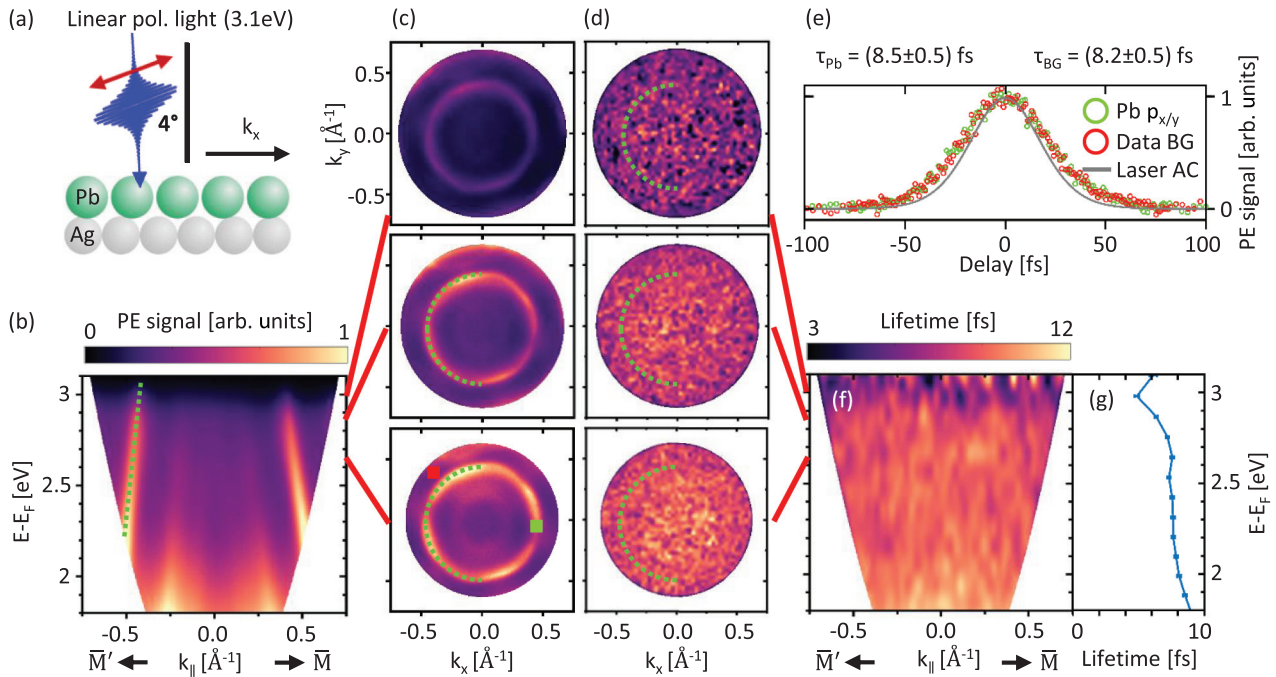


FIG. 2. Tr-2PMM data set of the Pb ML on Ag(111) system obtained with an incidence angle of 4° (nearly normal incidence) and a photon energy $\hbar\omega = 3.1$ eV [see panel (a)]. (b) E vs k_{\parallel} cut along the $\bar{M}'\bar{\Gamma}\bar{M}$ direction. Constant energy intensity (c) and lifetime (d) maps for $E-E_F = 2.65, 2.85,$ and 3.0 eV starting from the bottom to the top. (e) Exemplary autocorrelation traces of different regions in momentum space (dots) marked in (c), together with the two-pulse autocorrelation of the fs laser pulses (gray solid line). (f) Corresponding E vs k_{\parallel} lifetime map. (g) Energy-dependent quasiparticle lifetime obtained from the momentum averaged photoemission yield. In (b) and (d) The band dispersion of the Pb $p_{x/y}$ band is indicated with green dotted lines as a guide to the eye.

vector. This indicates that the observed electron dynamics only depends on the orientation of the electric field vector in the surface plane, but not on its specific orientation with respect to the high symmetry directions of the crystalline surface.

Next, we turn to our tr-2PMM data obtained for p-polarized light and a grazing incidence angle of 65° with respect to the surface normal [see sketch in Fig. 3(a)]. In this geometry, all Pb-derived states are now accessible in our 2PMM experiment due to the out-of-plane component of the electronic field vector of the pump and probe pulses. The remaining in-plane component of the electric field vector is oriented along the same in-plane high symmetry direction of the Pb/Ag(111) bilayer film as in the tr-2PMM experiment in normal incidence geometry discussed above. Hence, this ensures an almost identical excitation condition for Pb-derived states with in-plane character for both experimental geometries. The results are summarized in Figs. 3 and 4. The energy vs momentum cut through the unoccupied band structure along the $\bar{M}'\bar{\Gamma}\bar{M}$ direction in Fig. 3(b) reveals spectroscopic signatures of the QWS and the Pb $p_{x/y}$ band. Again, the dispersions of all states lead to characteristic emission patterns in the CE maps in Fig. 3(c), which were recorded at $E-E_F = 2.65, 2.85,$ and 3.0 eV. The Pb $p_{x/y}$ band reveals again a ringlike shape with azimuthal intensity distribution. In contrast, the predominant p_z orbital character of the Pb QWS results in a ringlike emission pattern with a marginal azimuthal intensity distribution. The quasiparticle lifetimes of these different states are reflected by their time-dependent autocorrelation traces. Exemplary normalized autocorrelation traces for se-

lected regions in energy- and momentum space are shown in Fig. 3(d) for the QWS (blue data points) as well as for the Pb $p_{x/y}$ band (green data points). As a reference, we also included an autocorrelation trace of the background signal of the photoemission yield (red data points). The fitting results of our autocorrelation analysis are superimposed onto the experimental data as black solid lines. The two-pulse correlation of the laser is included as gray solid line. For these exemplary regions in energy and momentum space, we find quasiparticle lifetimes of 10.9 and 10.1 fs for the QWS and the Pb $p_{x/y}$ band, respectively. These values are clearly distinguishable from the quasiparticle lifetime of the background signal within our relative uncertainty of <0.4 fs. This very small relative uncertainty between different energy- and momentum-space regions in a single experiment is due to the extremely high data quality. In particular, we find a very similar signal-to-noise ratio for all autocorrelation traces despite the significantly different photoemission yield in the different regions.

The quasiparticle lifetimes of the entire excited state band structure are summarized in the lifetime maps in Fig. 4. The CE maps in Fig. 4(a) reveal a disklike and a ringlike feature with quasiparticle lifetimes that are distinguishable from those of the homogeneous background of the Ag(111) crystal. Both features follow approximately the dispersion of the QWS (dashed circles) as well as of the Pb $p_{x/y}$ band (dotted circles) in all CE maps and hence reflect the momentum-dependent lifetimes of both states. The radius of the disklike feature in momentum space resembles very closely the energy-dependent band dispersion of the QWS

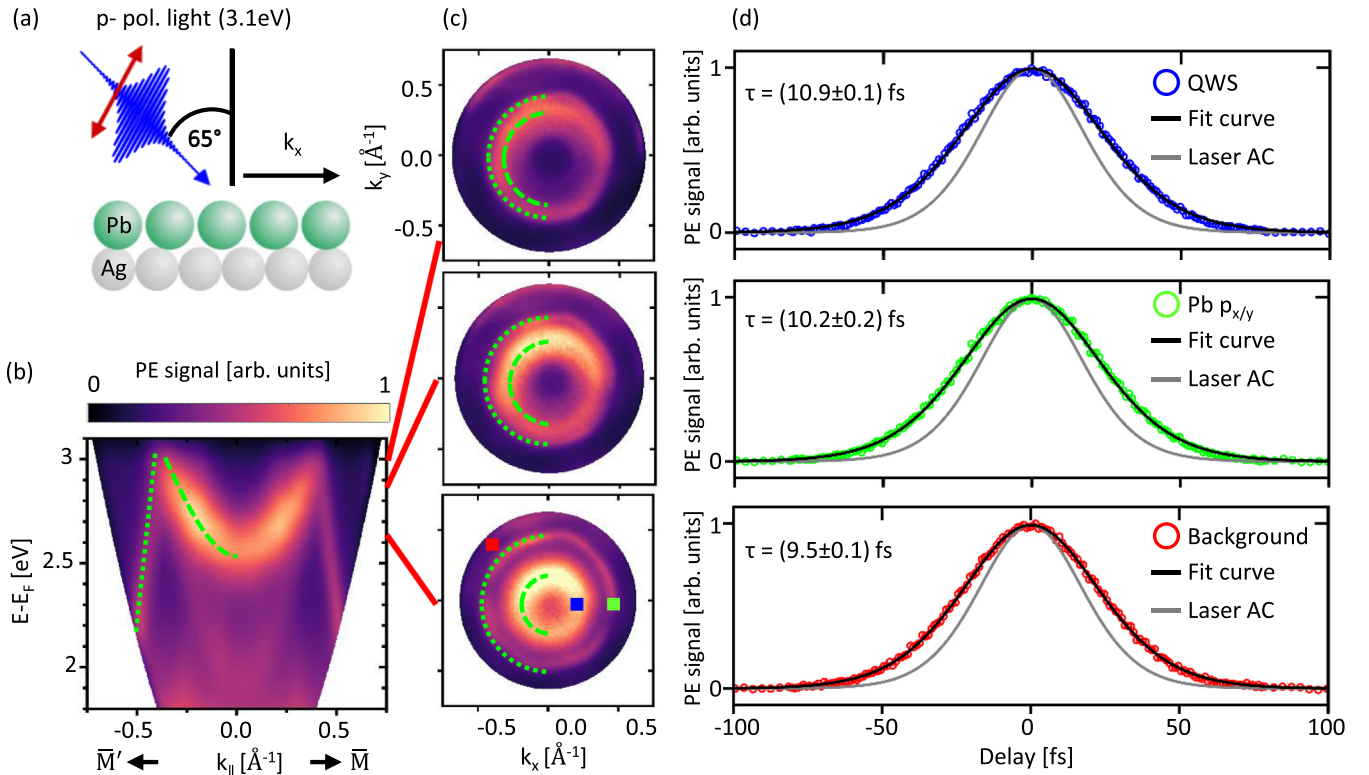


FIG. 3. Tr-2PMM data set of the Pb ML on Ag(111) system obtained in grazing incidence geometry (65° with respect to surface normal), p -polarized light, and $\hbar\omega = 3.1$ eV [see panel (a)]. (b) E vs k_{\parallel} cut along the $\bar{M}\bar{\Gamma}\bar{M}$ direction. Constant energy intensity (c) maps for $E - E_F = 2.65$, 2.85 , and 3.0 eV starting from the bottom to the top. The band dispersion of the Pb QWS and the Pb $p_{x/y}$ band are indicated by the green dashed and dotted lines that are guides to the eyes. (d) Exemplary autocorrelation traces for the quantum well state (blue), the Pb $p_{x/y}$ band (green) and the background (red). The corresponding regions are marked in (c). The data are shown as circles, the fit curve (black) and the laser cross correlation (grey) as solid lines.

as indicated by the dashed green circles in the CE lifetime maps in Fig. 4(a). This is even more clearly visible in the energy vs momentum lifetime map in Fig. 4(b), where the energy and momentum regions with distinct lifetimes resemble closely the parabolic dispersion of the QWS (green dashed curve). We observe a slight increase of the lifetime along its parabolic dispersion from $\tau \approx 12.0$ fs at $E - E_F = 3.0$ eV to $\tau \approx 13.2$ fs at $E - E_F = 2.7$ eV. Focusing more closely on the momentum-dependent lifetime of the QWS, we do not find any azimuthal variation for this state for all energies. However, the disk-like pattern of the QWS itself points to an additional (quasi-)elastic, but isotropic scattering process of electrons from the QWS towards the $\bar{\Gamma}$ point of the Brillouin zone. This additional momentum-dependent scattering mechanism is most likely responsible for the slight mismatch between the position of the QWS in energy and momentum and the regions of the largest quasiparticle lifetimes of the QWS.

The second feature with a distinct lifetime in the CE lifetime maps exhibits a ringlike pattern with an increasing radius for decreasing intermediate state energies. These energy-dependent radii resemble perfectly the dispersion of the Pb $p_{x/y}$ band (see green dotted line as a guide to the eye) as shown in the energy vs momentum lifetime map in Fig. 4(b). The lifetimes of this feature are between 10 and 11 fs for all energies and azimuthal orientations. This value is significantly larger than the lifetimes of the $p_{x/y}$ band obtained in normal incidence geometry. Hence this values cannot reflect

the intrinsic quasiparticle lifetime of the Pb $p_{x/y}$ band, which must be independent of the experimental geometry. Instead, the apparently different quasiparticle lifetime of the Pb $p_{x/y}$ band is the signature of a momentum-dependent refilling of electrons into the Pb $p_{x/y}$ band. We propose that this refilling process redistributes electrons from the QWS to the Pb $p_{x/y}$ band via an interband scattering process. Such an interband scattering process was already proposed for the QWS system Pb/Cu(111) [24]. Here, we additionally demonstrate the isotropic nature of the interband scattering processes in momentum space.

Altogether, the electron dynamics and the different inter- and intraband scattering processes are summarized in Fig. 4(c). Optically excited electrons in the QWS dissipate energy and momentum by isotropic intraband scattering following the band dispersion towards the band bottom of the QWS. Additional (quasi-)elastic scattering processes can isotropically redistribute electrons from the QWS either towards the center of the Brillouin zone, most likely by electron-defect scattering, or into the Pb $p_{x/y}$ band via interband scattering between both Pb-derived bands of different orbital character. Most importantly, only the interband scattering process from the QWS into the Pb $p_{x/y}$ band leads to an increased lifetime of the Pb $p_{x/y}$ band which otherwise vanishes for all energies and momenta accessible in our experiment. Hence, the electrons of the QWS act as an electron source for the isotropic interband

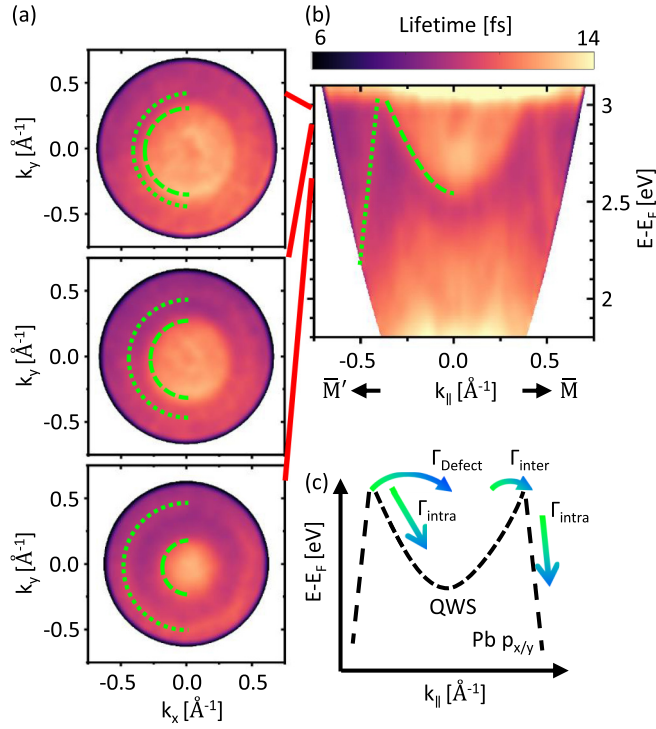


FIG. 4. Constant energy (a) and E vs k_{\parallel} lifetime maps (b) of the tr-2PMM data shown in Figs. 3(b) and 3(c). The band dispersion of the Pb QWS and the Pb $p_{x/y}$ band are indicated as green dashed and dotted lines, respectively. (c) Sketch of the inter- and intraband scattering processes dominating the hot electron dynamics of the Pb/Ag(111) bilayer system.

scattering processes observed for the Pb/Ag(111) bilayer system.

We now focus on the modifications of the ultrafast electron dynamics of the Pb/Ag(111) bilayer system after the adsorption of a highly ordered monolayer film of the aromatic molecule PTCDA [59]. Upon the adsorption of PTCDA on Pb/Ag(111), the Pb QWS is suppressed by the at least partial chemical interaction between PTCDA and the Pb layer [59]. Simultaneously, we observe a significant change in the overall shape of the autocorrelation traces which can no longer be modeled by a single autocorrelation curve by a single autocorrelation curve. This is illustrated in Fig. 5(a) which shows an exemplary momentum-averaged autocorrelation trace for a single intermediate state energy. The data were recorded with monochromatic radiation of 3.1 eV photon energy in grazing incidence geometry and p-polarized light pulses at room temperature. The experimental data are shown as black circles. The best fitting result for these data with a single autocorrelation curve calculated by optical Bloch equations is included as a black solid line. This model curve can no longer describe the line shape of the entire autocorrelation trace. In particular, we find clear deviations between the experimental data and the model curve for time delays between the pump and probe pulses larger than $\Delta t \approx 50$ fs. This underestimation of the experimental data by the modeled autocorrelation trace has already been observed for molecular adsorbates on surfaces and is a signature of an additional excited molecular state at this energy [33]. To consider both states in

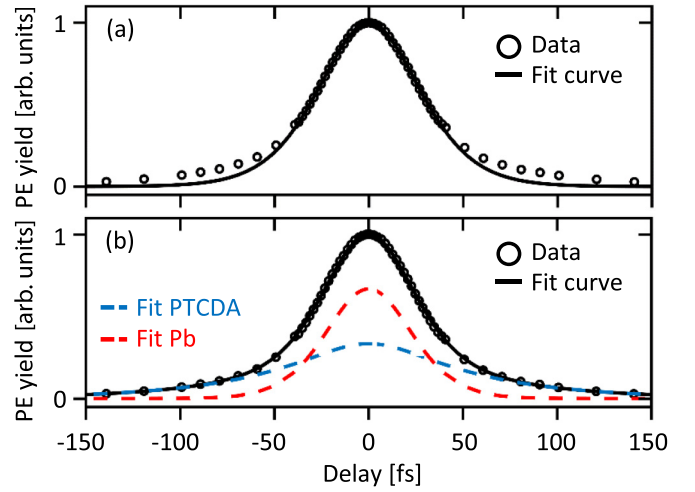


FIG. 5. Exemplary normalized autocorrelation curves extracted from the k -space integrated photoemission yield of a tr-2PMM experiment of the PTCDA/Pb/Ag(111) surface. As light source, a monochromatic laser setup with p -polarized light and 3.1 eV photon energy was used. The fits based on optical Bloch equations are plotted as black solid lines. The measured data in both panels are the same and presented as black circles. The data in panel (a) were fitted with one autocorrelation revealing a lifetime of $\tau = 14.1$ fs while the fit curve in region (b) is the sum of two separated autocorrelation curves, referring to the Pb and the PTCDA states. The autocorrelation trace of the PTCDA layers yields a lifetime of 50.2 fs and contributes 33% to the fitting envelope, the one of the Pb layer yields a lifetime of 8.3 fs with a weighting of 67% ($A = 0.33$).

our data analysis, we modelled the autocorrelation traces of the PTCDA/Pb/Ag(111) multilayer system $I_{2\text{PMM}}(k_x, k_y, E - E_F, \Delta t)$ at each point (k_x, k_y) in momentum space and for each energy $E - E_F$ with a linear combination of two autocorrelation traces $AC(\tau_i, \Delta t)$ exhibiting one lifetime $\tau_i = \tau_{\text{PTCDA}}$ for the molecular adsorbate states and one lifetime $\tau_i = \tau_{\text{Pb}}$ for the Pb-derived states:

$$I_{2\text{PMM}}(k_x, k_y, E - E_F, \Delta t) = A \times AC(\tau_{\text{PTCDA}}, \Delta t) + (1 - A) \times AC(\tau_{\text{Pb}}, \Delta t). \quad (1)$$

A and $(1 - A)$ are the weighting factors that model the relative contributions of both individual autocorrelation traces, with $A \in [0, 1]$. The fitting result of this model is shown in Fig. 5(b) as black solid line. The individual contributions of the metallic and the molecular states are included as red and blue dashed curves, respectively. The overall agreement of the fitting curve with the experimental data is excellent and we find a lifetime of $\tau_{\text{Pb}} = 8.3$ fs for the metallic state and of $\tau_{\text{PTCDA}} = 50.2$ fs for the molecular state. The weighting factor of the PTCDA contribution is $A = 0.33$.

The same model is used to determine the momentum-dependent lifetimes of the molecular and Pb-derived states which are shown in Fig. 6. This approach results in individual CE lifetime maps for the molecular and the substrate states. To increase the reliability of our fitting procedure, we fixed the weighting factor A for each energy to a constant value, i.e., the only free fitting parameters are the quasiparticle lifetimes τ_{PTCDA} and τ_{Pb} . The energy-dependent weighting factor was

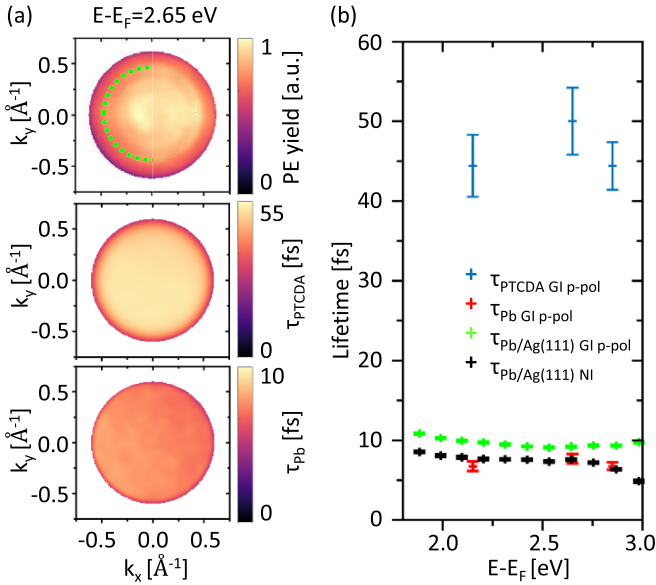


FIG. 6. Tr-2PMM data of a PTCDA monolayer film on a Pb/Ag(111) bilayer (p -polarized light, grazing incidence, $\hbar\omega = 3.1$ eV). (a) CE intensity and lifetime maps of the PTCDA and Pb derived states for $E-E_F = 2.65$ eV. (b) Momentum averaged lifetimes of PTCDA (red) and Pb (blue) -derived states of the PTCDA/Pb/Ag(111) multilayer structure. As a reference, the momentum averaged lifetimes of the bare Pb/Ag(111) bilayer are depicted in green and black for grazing (GI, p -pol) and normal incidence (NI) geometry.

determined separately by analyzing the autocorrelation trace of the momentum integrated photoemission yield using A as a free fitting parameter. CE intensity maps (top) as well as the lifetime maps of the PTCDA- (middle) and Pb-derived states (bottom) are exemplarily shown for an intermediate state energy of $E-E_F = 2.65$ eV in Fig. 6(a). The CE intensity map reveals a ring with azimuthal intensity modulation which can be attributed to the Pb $p_{x/y}$ band (dotted line). The other features refer to bands from the occupied part of the band structure.

Despite this well-defined emission pattern of the highly ordered PTCDA/Pb/Ag(111) multilayer structure, the CE lifetime maps of the molecular and Pb-derived states only reveal a homogeneous distribution of lifetimes for all accessible momenta. This might not be surprising for the molecular states. They typically exhibit their main characteristic momentum space signatures for much larger momenta that are inaccessible in our tr-2PMM experiment [59,66,76–79]. For small electron momenta, their signal is dominated by the tails of these main maxima, which do not reveal such clear emission maxima in momentum space. However, we also do not observe any signature of a ringlike feature of the Pb-derived $p_{x/y}$ band as found for the CE lifetime map of the bare Pb/Ag(111) bilayer system for identical excitation conditions (see Fig. 4). This directly points to a suppression of any refilling processes of electrons into the Pb $p_{x/y}$ band due to the adsorption of PTCDA.

Similar results were obtained for the intermediate state energies $E-E_F = 2.15$ eV and $E-E_F = 2.85$ eV. In particular, no signatures of the band dispersion of the Pb $p_{x/y}$ band can

be observed in the CE lifetime maps of the Pb-derived bands for any energy. These homogeneous lifetime distributions in all CE lifetime maps allow us to summarize the momentum-independent lifetime for the molecular and Pb-derived states in Fig. 6(b). The corresponding momentum-integrated lifetimes of the bare Pb/Ag(111) bilayer systems for excitation in normal and grazing incidence geometry are included as black and green dots, respectively. For the PTCDA/Pb/Ag(111) system, we find lifetimes of $\tau_{\text{PTCDA}} \approx 45$ fs for the molecular state and of $\tau_{\text{Pb}} \approx 8$ fs for the Pb-derived signals for all energies. The lifetimes in the energy range of the molecular state of PTCDA on the Pb surface are comparable to previous studies of molecular materials on metallic surfaces [80]. Interestingly, the lifetimes of the Pb-derived states reflect more closely the lifetimes determined for the bare Pb/Ag(111) bilayer system in normal incidence geometry, and not with those lifetimes determined in identical, grazing incidence geometry. This observation is mainly due to the absence of the refilling processes into the Pb $p_{x/y}$ band. It hence supports our previous conclusion that the Pb QWS acts as an electron source for all isotropic momentum space scattering processes in the Pb/Ag(111) bilayer system.

Interestingly, our experimental data do not reveal any signature of an electron transfer from the molecular into the Pb layer underneath. In particular, the molecular state in the energy range of the Pb QWS cannot act as an electron source for the refilling of the Pb $p_{x/y}$ band. This points to a rather weak coupling between the p_z -like orbitals of the excited molecular states and the $p_{x/y}$ -like orbitals of the Pb $p_{x/y}$ band. This observation is particularly interesting since the adsorption of PTCDA on the Pb layer suppresses the Pb QWS due to an at least partial chemical interaction at the interface [59]. Both findings can only be explained by an orbital-selective interaction across the interface that strongly depends on the spatial overlap between the corresponding molecular and Pb states at the interface. Such an orbital-selective hybridizing was already reported for the Pb/Ag(111) interface and resulted in an orbital-dependent broadening of the Pb valence bands [58]. For the PTCDA/Pb interface, we propose that the large spatial overlap and the correspondingly strong interaction between the p_z -like orbitals of PTCDA and the Pb QWS are responsible for the suppression of the Pb QWS. In contrast, the marginal overlap between the p_z orbitals of the excited molecular states and the $p_{x/y}$ orbitals of the Pb band results in a marginal coupling between these states. This small coupling prevents an efficient interfacial charge transfer between molecular and Pb-derived states at the PTCDA/Pb interface.

IV. SUMMARY AND CONCLUSION

In our work, we have investigated the momentum-dependent electron dynamics of the quantum well system of one layer Pb on Ag(111) prior and after the adsorption of PTCDA using tr-2PMM in different excitation geometries. The hot electron dynamics of the bare Pb/Ag(111) bilayer system is determined by two different scattering processes that we find to be isotropic in momentum space. The electrons of the p_z -like QWS dissipate energy and momentum via isotropic intraband scattering leading to an increase of the quasiparticle lifetime from 12 fs to 13.2 fs from the highest

accessible intermediate state energy towards the band bottom of the parabolic QWS. In addition, we find signatures of an isotropic (quasi-)elastic interband scattering process of electrons from the QWS into a Pb $p_{x/y}$ band. This refilling process leads to a non-vanishing lifetime of the Pb $p_{x/y}$ band with otherwise neglectable intrinsic quasiparticle lifetime. This clearly shows that the Pb QWS acts as an electron source for the isotropic momentum-dependent scattering processes of the Pb/Ag(111) bilayer system.

This conclusion is fully supported by the hot electron dynamics of PTCDA on Pb/Ag(111) where the partially chemical interaction between PTCDA and the Pb layer suppresses the Pb QWS. This band structure modification prevents any refilling and momentum-dependent interband scattering of electrons within the Pb layer and hence results in a neglectable quasiparticle lifetime of the Pb $p_{x/y}$ band. In addition, we find indications of an excited molecular state in the energy range of the Pb $p_{x/y}$ band with a quasiparticle lifetime of $\tau_{\text{PTCDA}} \approx 45$ fs for all energies.

Altogether, our investigation of a highly symmetric and low dimensional metallic bilayer systems has demonstrated the important role of isotropic inter- and intraband scattering processes for the momentum-dependent hot electron

dynamics of excited states with different orbital characters. Moreover, our study demonstrated a clear link between the adsorption-induced modification of the excited state band structure and the corresponding hot electron dynamics of the metallic bilayer system. These are the first crucial steps towards controlling scattering processes of low dimensional systems and quantum (well) materials by the adsorption of organic molecules.

ACKNOWLEDGMENTS

The experimental work was funded by the Deutsche Forschungsgemeinschaft (DFG, German Research Foundation) - TRR 173 - 268565370 Spin + X: spin in its collective environment (Projects A02 and B05). F.H. acknowledges financial support from the Graduate School of Excellence MAINZ (Excellence Initiative DFG/GSC 266), B.S. by the Dynamics and Topology Center funded by the State of Rhineland Palatinate. M.C. acknowledges funding from the European Research Council (ERC) under the European Union's Horizon 2020 research and innovation programme (Grant Agreement No. 725767- hyControl).

-
- [1] M. Cinchetti, V. A. Dediu, and L. E. Hueso, *Nat. Mater.* **16**, 507 (2017).
- [2] T.-C. Chiang, *Surf. Sci. Rep.* **39**, 181 (2000).
- [3] J. C. R. Sánchez, L. Vila, G. Desfonds, S. Gambarelli, J. P. Attané, J. M. de Teresa, C. Magén, and A. Fert, *Nat. Commun.* **4**, 2944 (2013).
- [4] M. Isasa, M. C. Martínez-Velarte, E. Villamor, C. Magen, L. Morellon, J. M. DeTeresa, M. R. Ibarra, G. Vignale, E. V. Chulkov, E. E. Krasovskii, L.E. Hueso, and F. Casanova, *Phys. Rev. B* **93**, 014420 (2016).
- [5] S. Oyarzún, A. K. Nandy, F. Rortais, J.-C. Rojas-Sánchez, M.-T. Dau, P. Noël, P. Laczkowski, S. Pouget, H. Okuno, L. Vila *et al.*, *Nat. Commun.* **7**, 13857 (2016).
- [6] I. Bergenti and V. Dediu, *Nano Mater. Sci.* **1**, 149 (2019).
- [7] T. Valla, A. V. Fedorov, P. D. Johnson, and S. L. Hulbert, *Phys. Rev. Lett.* **83**, 2085 (1999).
- [8] M. Ligges, M. Sandhofer, I. Sklyadneva, R. Heid, K.-P. Bohnen, S. Freutel, L. Rettig, P. Zhou, P. M. Echenique, E. V. Chulkov *et al.*, *J. Phys. Condens. Matter.* **26**, 352001 (2014).
- [9] F. Reinert, B. Eltner, G. Nicolay, D. Ehm, S. Schmidt, and S. Hüfner, *Phys. Rev. Lett.* **91**, 186406 (2003).
- [10] B. A. McDougall, T. Balasubramanian, and E. Jensen, *Phys. Rev. B* **51**, 13891(R) (1995).
- [11] J. Li, W.-D. Schneider, R. Berndt, O. R. Bryant, and S. Crampin, *Phys. Rev. Lett.* **81**, 4464 (1998).
- [12] L. Bürgi, O. Jeandupeux, H. Brune, and K. Kern, *Phys. Rev. Lett.* **82**, 4516 (1999).
- [13] H. Jensen, J. Kröger, R. Berndt, and S. Crampin, *Phys. Rev. B* **71**, 155417 (2005).
- [14] J. Kliewer, R. Berndt, E. V. Chulkov, V. M. Silkin, P. M. Echenique, and S. Crampin, *Science* **288**, 1399 (2000).
- [15] F. J. Himpsel, *Surf. Rev. Lett.* **02**, 81 (1995).
- [16] M. Bauer, S. Pawlik, and M. Aeschlimann, *Phys. Rev. B* **55**, 10040 (1997).
- [17] S. Ogawa, H. Nagano, and H. Petek, *Phys. Rev. Lett.* **88**, 116801 (2002).
- [18] E. V. Chulkov, J. Kliewer, R. Berndt, V. M. Silkin, B. Hellsing, S. Crampin, and P. M. Echenique, *Phys. Rev. B* **68**, 195422 (2003).
- [19] D. Wegner, A. Bauer, and G. Kaindl, *Phys. Rev. Lett.* **94**, 126804 (2005).
- [20] P. S. Kirchmann and U. Bovensiepen, *Phys. Rev. B* **78**, 035437 (2008).
- [21] M. Cinchetti, K. Heimer, J.-P. Wüstenberg, O. Andreyev, M. Bauer, S. Lach, C. Ziegler, Y. Gao, and M. Aeschlimann, *Nat. Mater.* **8**, 115 (2009).
- [22] A. Zugarramurdi, N. Zabala, V. M. Silkin, A. G. Borisov, and E. V. Chulkov, *Phys. Rev. B* **80**, 115425 (2009).
- [23] I. Hong, C. Brun, F. Patthey, I. Y. Sklyadneva, X. Zubizarreta, R. Heid, V. M. Silkin, P. M. Echenique, K. P. Bohnen, E. V. Chulkov, and W. D. Schneider, *Phys. Rev. B* **80**, 081409(R) (2009).
- [24] S. Mathias, A. Ruffing, F. Deicke, M. Wiesenmayer, M. Aeschlimann, and M. Bauer, *Phys. Rev. B* **81**, 155429 (2010).
- [25] S. Link, A. Scholl, R. Jacquemin, and W. Eberhardt, *Solid State Commun.* **113**, 689 (2000).
- [26] X. Zhu, *Surf. Sci. Rep.* **56**, 1 (2004).
- [27] G. Dutton, D. P. Quinn, C. D. Lindstrom, and X.-Y. Zhu, *Phys. Rev. B* **72**, 045441 (2005).
- [28] J. Güdde, W. Berthold, and U. Höfer, *Chem. Rev.* **106**, 4261 (2006).
- [29] L. Gundlach, R. Ernstorfer, and F. Willig, *Appl. Phys. A* **88**, 481 (2007).
- [30] A. Hotzel, *Prog. Surf. Sci.* **82**, 336 (2007).

- [31] S. Hagen, Y. Luo, R. Haag, M. Wolf, and P. Tegeder, *New J. Phys.* **12**, 125022 (2010).
- [32] A. Zugarramurdi, N. Zabala, V. M. Silkin, E. V. Chulkov, and A. G. Borisov, *Phys. Rev. B* **86**, 075434 (2012).
- [33] S. Steil, N. Großmann, M. Laux, A. Ruffing, D. Steil, M. Wiesenmayer, S. Mathias, O. L. A. Monti, M. Cinchetti, and M. Aeschlimann, *Nat. Phys.* **9**, 242 (2013).
- [34] A. Droghetti, P. Thielen, I. Rungger, N. Haag, N. Großmann, J. Stöckl, B. Stadtmüller, M. Aeschlimann, S. Sanvito, and M. Cinchetti, *Nat. Commun.* **7**, 12668 (2016).
- [35] B. Stadtmüller, S. Emmerich, D. Jungkenn, N. Haag, M. Rollinger, S. Eich, M. Maniraj, M. Aeschlimann, M. Cinchetti, and S. Mathias, *Nat. Commun.* **10**, 1470 (2019).
- [36] C. A. Schmuttenmaer, M. Aeschlimann, H. E. Elsayed-Ali, R. J. D. Miller, D. A. Mantell, J. Cao, and Y. Gao, *Phys. Rev. B* **50**, 8957 (1994).
- [37] M. Wolf, *Surf. Sci.* **377-379**, 343 (1997).
- [38] H. Petek and S. Ogawa, *Prog. Surf. Sci.* **56**, 239 (1997).
- [39] M. Weinelt, *J. Phys.: Condens. Matter* **14**, R1099 (2002).
- [40] K. Boger, T. Fauster, and M. Weinelt, *New J. Phys.* **7**, 110 (2005).
- [41] U. Bovensiepen and P. S. Kirchmann, *Laser Photonics Rev.* **6**, 589 (2012).
- [42] M. Bauer, A. Marienfeld, and M. Aeschlimann, *Prog. Surf. Sci.* **90**, 319 (2015).
- [43] M. Lisowski, P. A. Loukakos, U. Bovensiepen, and M. Wolf, *Appl. Phys. A* **79**, 739 (2004).
- [44] D. Gerbert and P. Tegeder, *Phys. Rev. B* **96**, 144304 (2017).
- [45] W. Berthold, U. Höfer, P. Feulner, E. V. Chulkov, V. M. Silkin, and P. M. Echenique, *Phys. Rev. Lett.* **88**, 056805 (2002).
- [46] K. Boger, M. Weinelt, and T. Fauster, *Phys. Rev. Lett.* **92**, 126803 (2004).
- [47] J. Güdde, M. Rohleder, T. Meier, S. W. Koch, and U. Höfer, *Science* **318**, 1287 (2007).
- [48] A. S. Syed, V. M. Trontl, M. Ligges, S. Sakong, P. Kratzer, D. Lükermann, P. Zhou, I. Avigo, H. Pfnür, C. Tegenkamp *et al.*, *Phys. Rev. B* **92**, 134301 (2015).
- [49] C. Monney, M. Puppini, C. W. Nicholson, M. Hoesch, R. T. Chapman, E. Springate, H. Berger, A. Magrez, C. Cacho, R. Ernstorfer, and M. Wolf, *Phys. Rev. B* **94**, 165165 (2016).
- [50] S. Aeschlimann, R. Krause, M. Chávez-Cervantes, H. Bromberger, R. Jago, E. Malić, A. Al-Temimy, C. Coletti, A. Cavalleri, and I. Gierz, *Phys. Rev. B* **96**, 020301(R) (2017).
- [51] A. S. Ketterl, S. Otto, M. Bastian, B. Andres, C. Gahl, J. Minár, H. Ebert, J. Braun, O. E. Tereshchenko, K. A. Kokh, Th. Fauster, and M. Weinelt, *Phys. Rev. B* **98**, 155406 (2018).
- [52] M. Weinelt, A. B. Schmidt, M. Pickel, and M. Donath, *Prog. Surf. Sci.* **82**, 388 (2007).
- [53] M. Marks, A. Schöll, and U. Höfer, *J. Electron Spectrosc.* **195**, 263 (2014).
- [54] C. H. Schwalb, S. Sachs, M. Marks, A. Schöll, F. Reinert, E. Umbach, and U. Höfer, *Phys. Rev. Lett.* **101**, 146801 (2008).
- [55] S. Mathias, M. Wiesenmayer, M. Aeschlimann, and M. Bauer, *Phys. Rev. Lett.* **97**, 236809 (2006).
- [56] R. Bertoni, C.W. Nicholson, L. Waldecker, H. Hubener, C. Monney, U. DeGiovannini, M. Puppini, M. Hoesch, E. Springate, R.T. Chapman, C. Cacho, M. Wolf, A. Rubio, and R. Ernstorfer, *Phys. Rev. Lett.* **117**, 277201 (2016).
- [57] K. Kuroda, J. Reimann, J. Gudde, and U. Höfer, *Phys. Rev. Lett.* **116**, 076801 (2016).
- [58] C. R. Ast, D. Pacilé, M. Papagno, T. Gloor, F. Mila, S. Fedrigo, G. Wittich, K. Kern, H. Brune, and M. Grioni, *Phys. Rev. B* **73**, 245428 (2006).
- [59] B. Stadtmüller, L. Grad, J. Seidel, F. Haag, N. Haag, M. Cinchetti, and M. Aeschlimann, *J. Phys.: Condens. Matter* **31**, 134005 (2019).
- [60] F. Haag, T. Eul, P. Thielen, N. Haag, B. Stadtmüller, and M. Aeschlimann, *Rev. Sci. Instrum.* **90**, 103104 (2019).
- [61] M. Escher, N. Weber, M. Merkel, C. Ziethen, P. Bernhard, G. Schönhense, S. Schmidt, F. Forster, F. Reinert, B. Krömker *et al.*, *J. Phys.: Condens. Matter* **17**, S1329 (2005).
- [62] B. Krömker, M. Escher, D. Funnemann, D. Hartung, H. Engelhard, and J. Kirschner, *Rev. Sci. Instrum.* **79**, 053702 (2008).
- [63] C. Tusche, A. Krasnyuk, and J. Kirschner, *Ultramicroscopy* **159**, 520 (2015).
- [64] G. Schönhense, K. Medjanik, C. Tusche, M. de Loos, B. van der Geer, M. Scholz, F. Hieke, N. Gerken, J. Kirschner, and W. Wurth, *Ultramicroscopy* **159**(Pt 3), 488 (2015).
- [65] L. Kilian, E. Umbach, and M. Sokolowski, *Surf. Sci.* **573**, 359 (2004).
- [66] B. Stadtmüller, M. Willenbockel, E. M. Reinisch, T. Ules, F. C. Bocquet, S. Soubatch, P. Puschnig, G. Koller, M. G. Ramsey, F. S. Tautz *et al.*, *EPL (Europhysics Letters)* **100**, 26008 (2012).
- [67] A. Oelsner, O. Schmidt, M. Schicketanz, M. Klais, G. Schönhense, V. Mergel, O. Jagutzki, and H. Schmidt-Böcking, *Rev. Sci. Instrum.* **72**, 3968 (2001).
- [68] A. Oelsner, M. Rohmer, C. Schneider, D. Bayer, G. Schönhense, and M. Aeschlimann, *J. Electron Spectrosc.* **178-179**, 317 (2010).
- [69] T. Hertel, E. Knoesel, M. Wolf, and G. Ertl, *Phys. Rev. Lett.* **76**, 535 (1996).
- [70] F. Steeb, S. Mathias, A. Fischer, M. Wiesenmayer, M. Aeschlimann, and M. Bauer, *New J. Phys.* **11**, 013016 (2009).
- [71] P. Kahl, S. Wall, C. Witt, C. Schneider, D. Bayer, A. Fischer, P. Melchior, M. Horn-von Hoegen, M. Aeschlimann, and F.-J. Meyer zu Heringdorf, *Plasmonics* **9**, 1401 (2014).
- [72] M. Aeschlimann, M. Bauer, and S. Pawlik, *Chem. Phys.* **205**, 127 (1996).
- [73] S. Ogawa, H. Nagano, and H. Petek, *Phys. Rev. B* **55**, 10869 (1997).
- [74] G. D. Mahan, *Phys. Rev. B* **2**, 4334 (1970).
- [75] A. Winkelmann, A. Akin Ünal, C. Tusche, M. Ellguth, C.-T. Chiang, and J. Kirschner, *New J. Phys.* **14**, 083027 (2012).
- [76] P. Puschnig, S. Berkebile, A. J. Fleming, G. Koller, K. Emtsev, T. Seyller, J. D. Riley, C. Ambrosch-Draxl, F. P. Netzer, and M. G. Ramsey, *Science* **326**, 702 (2009).
- [77] J. Ziroff, F. Forster, A. Schöll, P. Puschnig, and F. Reinert, *Phys. Rev. Lett.* **104**, 233004 (2010).
- [78] G. S. M. Jansen, M. Keunecke, M. Düvel, C. Möller, D. Schmitt, W. Bennecke, F. J. S. Kappert, D. Steil, D. R. Luke, S. Steil *et al.*, *New J. Phys.* **22**, 063012 (2020).
- [79] R. Wallauer, M. Raths, K. Stallberg, L. Münster, D. Brandstetter, X. Yang, J. Güdde, P. Puschnig, S. Soubatch, C. Kumpf *et al.*, *Science* **371**, 1056 (2021).
- [80] C. H. Schwalb, M. Marks, S. Sachs, A. Schöll, F. Reinert, E. Umbach, and U. Höfer, *Eur. Phys. J. B* **75**, 23 (2010).